Open questions about homogeneous fluid dynamos: The VKS experiment

L. Marié, F. Pétrélis, M. Bourgoin, J. Burguete, A. Chiffaudel, F. Daviaud, S Fauve, P. Odier, J.-F. Pinton

MAGNETOHYDRODYNAMICS Vol. 38 (2002), No. 1-2, pp. 163–176

OPEN QUESTIONS ABOUT HOMOGENEOUS FLUID DYNAMOS: THE VKS EXPERIMENT

L. Marié[1], *F. Pétrélis*[2], *M. Bourgoin*[3], *J. Burguete*[1,4], *A. Chiffaudel*[1], *F. Daviaud*[1], *S. Fauve*[1], *P. Odier*[2], *J.-F. Pinton*[2]

[1] *Service de Physique de l'Etat Condensé, DSM/DRECAM, CEA/Saclay, 91191 Gif-sur-Yvette cedex, France*
[2] *Laboratoire de Physique Statistique de l'Ecole Normale Supérieure, CNRS UMR 8550, 24 Rue Lhomond, 75231 Paris cedex 05, France;*
[3] *Laboratoire de Physique de l'Ecole Normale Supérieure de Lyon, CNRS UMR 5672, 46 allée d'Italie, 69364 Lyon cedex 07, France;*
[4] *Present address: Departamento de Física y Matemática Aplicada, Universidad de Navarra, E-31080 Pamplona, Spain*

We consider several problems that arise in the context of homogeneous fluid dynamos such as the effect of turbulence on the dynamo threshold, the saturation level of the generated magnetic field above the threshold and its dynamics. We compare some of our predictions with the recent experimental results of the Karlsruhe and Riga experiments. Finally, we present the VKS experiment that we have designed to answer some of the remaining open questions. We study, in particular, the response of a turbulent flow to an external magnetic field.

Introduction. Decades after the discovery of the first analytical examples of laminar fluid dynamos [1, 2, 3, 4], the self-generation of a magnetic field by a flow of liquid sodium has been reported by the Karlsruhe [5] and Riga [6] groups. Although there were no doubts about self-generation by the laminar Roberts type [3] or Ponomarenko type [4] flows that were used, these experiments are major steps in the study of the dynamo problem because they have raised several interesting questions.

As already mentioned by these groups and by several other groups [7, 8] who studied these experimental configurations, the observed thresholds are in rather good agreement with the theoretical predictions made by considering only the laminar mean flow and neglecting the small-scale turbulent fluctuations that are present in both experiments. There are no a priori reasons that the growth of the magnetic field should be primarily governed by the mean flow, and dynamo models using turbulent fluctuations with a zero mean flow have been known for a long time [9, 10]. The problem of the effect of turbulent fluctuations on the dynamo threshold thus remains to be understood. This shows that there are still open questions even at the level of the kinematic dynamo problem.

The saturation level of the magnetic field due to the back reaction of the Lorentz force on the flow has been measured in the Karlsruhe and Riga experiments and is discussed in the present volume (see e.g. Gailitis *et al.* , Tilgner *et al.* , Rädler *et al.*) and in reference [11]. Different scaling laws have been found theoretically using mean-field electrodynamics [12, 13, 14] or perturbation theory close to the dynamo threshold for laminar flows [13, 15, 16, 17, 18, 19, 20, 21]. It has been shown recently that, although laminar models correctly predict the dynamo threshold in the Karlsruhe and Riga experiments, they do not give even a rough order of magnitude of the value of the saturation magnetic field above the

threshold; on the contrary, a scaling law taking into account turbulence is in much better agreement [22].

The dynamics of the generated magnetic field is another important aspect of fluid dynamos. Field reversals have not been observed in the Karlsruhe and Riga experiments. This may be related to the fact that the large scales of the flow are geometrically constrained in these experiments. The possibility of reversals should be studied with dynamo experiments in unconstrained geometries. Some statistical features of the fluctuations of the generated magnetic field have been studied in the Karlsruhe experiment. They can be compared to the ones reported in the experiments performed below the dynamo threshold but with an applied external magnetic field [23, 24] and appear to be very similar to the results of the VKS experiment [24]. It would be of great interest to show that the properties of the small-scale fluctuations result only from the chaotic advection of a large-scale magnetic field by the turbulent flow, whether this field is self-generated just above the dynamo threshold or externally applied.

1. Governing equations and dimensional arguments. The equations governing the magnetic and velocity fields, $\mathbf{B}(\mathbf{r},t)$ and $\mathbf{V}(\mathbf{r},t)$, in the MHD approximation are

$$\nabla \cdot \mathbf{B} = 0, \tag{1}$$

$$\frac{\partial \mathbf{B}}{\partial t} = \nabla \times (\mathbf{V} \times \mathbf{B}) + \frac{1}{\mu_0 \sigma} \Delta \mathbf{B}, \tag{2}$$

$$\nabla \cdot \mathbf{V} = 0, \tag{3}$$

$$\frac{\partial \mathbf{V}}{\partial t} + (\mathbf{V} \cdot \nabla)\mathbf{V} = -\frac{1}{\rho} \nabla \left(p + \frac{B^2}{2\mu_0} \right) + \nu \Delta \mathbf{V} + \frac{1}{\mu_0 \rho} (\mathbf{B} \cdot \nabla)\mathbf{B}, \tag{4}$$

where $p(\mathbf{r},t)$ is the pressure field, μ_0 is the magnetic permeability of vacuum, σ is the electric conductivity, ν is the kinematic viscosity and ρ is the density of the fluid. We can define two independent dimensionless numbers, the magnetic Reynolds number, $\mathrm{Rm} = \mu_0 \sigma L U$, with a characteristic velocity U of the solid boundaries driving the fluid motion and characteristic integral scale L of the flow, and the magnetic Prandtl number, $\mathrm{Pm} = \mu_0 \sigma \nu$. We have thus $\mathrm{Rm} = \mathrm{RePm}$, where $\mathrm{Re} = LU/\nu$ is the kinetic Reynolds number of the flow. For most of the known fluid dynamos, the dynamo threshold $\mathrm{Rm_c}$ is roughly in the range $10 \ldots 100$. For liquid metals, $\mathrm{Pm} < 10^{-5}$, thus the kinetic Reynolds number at dynamo onset is larger than 10^6 and, consequently, the flow is strongly turbulent. In the limit of a very large kinetic Reynolds number, a dimensional argument gives the power needed to maintain the flow [25]:

$$P = K_\mathrm{P} \rho L^2 U^3 \tag{5}$$

where K_P is a dimensionless factor that depends on the geometry of the container and the shape of the propellers. We can write the magnetic Reynolds number as:

$$\mathrm{Rm} = \mu_0 \sigma \left(\frac{PL}{K_\mathrm{P} \rho} \right)^{1/3}. \tag{6}$$

This last formula has simple consequences: first, taking liquid sodium (the liquid metal with the highest electric conductivity), $\mu_0 \sigma \sim 10\,\mathrm{m^{-2}s}$, $\rho \sim 10^3\,\mathrm{kgm^{-3}}$, $K_\mathrm{P} \sim 0.1$ (see Section 5) and a typical lengthscale $L \sim 1$ m, we get $P = 0.1\mathrm{Rm}^3$; thus a mechanical power of the order of 100 kW is needed to reach a dynamo threshold of the order of 100. Second, experimental dynamos operating at large

Rm compared with $\mathrm{Rm_c}$ are hardly possible: it costs almost 10 times more power to reach $2\mathrm{Rm_c}$ from the dynamo threshold. In conclusion, most experimental dynamos should have the following characteristics:

(i) they bifurcate from a strongly turbulent flow regime;

(ii) they operate in the vicinity of their bifurcation threshold.

Although (i) makes any realistic analytical calculation or direct numerical simulation almost impossible, we will show below, using the dimensional analysis, that the above two characteristics allow an estimate of the nonlinear saturated mean value of the magnetic field above $\mathrm{Rm_c}$.

2. Turbulence and the dynamo threshold. As said above, small-scale turbulent fluctuations are present in the Karlsruhe and Riga experiments. However, they do not affect the dynamo threshold, which is in agreement with the one computed for a laminar flow with a velocity field $\langle \mathbf{V}(\mathbf{r}) \rangle$, where $\langle\,\rangle$ stands for the average in time. This is unlikely to be the case with unconstrained turbulent flows, for which the instantaneous velocity field $\mathbf{V}(\mathbf{r},t)$ strongly differs from $\langle \mathbf{V}(\mathbf{r}) \rangle$ even at large scales. Writing $\mathbf{V}(\mathbf{r},t) = \langle \mathbf{V}(\mathbf{r}) \rangle + \mathbf{v}(\mathbf{r},t)$, the problem is to study the effect of the fluctuating velocity field $\mathbf{v}(\mathbf{r},t)$ on the dynamo mechanisms. We get from (2) for the kinematic dynamo problem:

$$\frac{\partial \mathbf{B}}{\partial t} = \nabla \times (\langle \mathbf{V} \rangle \times \mathbf{B}) + \nabla \times (\mathbf{v} \times \mathbf{B}) + \frac{1}{\mu_0 \sigma} \Delta \mathbf{B}. \tag{7}$$

For small fluctuations $\mathbf{v}(\mathbf{r},t)$, turbulence may just act as a random multiplicative forcing, thus shifting the laminar dynamo threshold and modifying the dynamics of the self-generated field in the threshold vicinity. As in other experimentally studied instability problems, the multiplicative random forcing may generate intermittent bursting in the vicinity of instability onset [26, 27]. This type of behavior, understood in the framework of blowout bifurcations in dynamical system theory, has been observed in a numerical simulation of the MHD equations [28]. In these simulations, Pm was of order one, and the flow was chaotic at the dynamo threshold but not fully turbulent.

As said above, in experiments with unconstrained flows, one expects fully developed turbulent fluctuations at all scales. It is probable that the observed dynamo strongly differs from the one computed as if it were generated by $\langle \mathbf{V}(\mathbf{r}) \rangle$ alone. Indeed, there exist even simple phenomenological models of dynamos generated only by turbulent fluctuations, i.e., with $\langle \mathbf{V}(\mathbf{r}) \rangle = 0$ [10]. It is thus of great interest to study the effect of turbulent fluctuations on the dynamo problem in a flow without geometrical constraints and to observe a situation, where self-generation is primarily due to turbulent fluctuations. From the fundamental and mathematical viewpoints, the problem is to understand how a coherent field $\langle \mathbf{B}(\mathbf{r}) \rangle$ is amplified by a random velocity field in order to test the validity of mean field models, and to study the statistical properties of field fluctuations. In an astrophysical context, the turbulent dynamos are also likely to be the relevant ones in most situations.

The role of turbulent fluctuations at large Reynolds numbers may be twofold: on one hand, they decrease the effective electrical conductivity and thus inhibits the dynamo action generated by $\langle \mathbf{V}(\mathbf{r}) \rangle$ by increasing Joule dissipation [29]. On the other hand, they may generate a large scale magnetic field through the "α-effect" or higher order similar effects [9, 10, 30, 31], even if $\langle \mathbf{V}(\mathbf{r}) \rangle = 0$. Consequently, there may also exist a parameter range, in which the threshold of the dynamo related to the mean flow alone is decreased by turbulent fluctuations. The problem can thus be stated as follows: for a given driving of the flow, what is the dependence of the critical magnetic Reynolds number for dynamo onset, $\mathrm{Rm_c}$, as a function of

the magnetic Prandtl number or equivalently as a function of the kinetic Reynolds number of the flow? In particular, is it possible to predict the behavior of $\mathrm{Rm_c}$ within the limit of infinite kinetic Reynolds number, at least for some class of flow drivings? Experiments are the only way to give a clear answer to this question because direct numerical simulations cannot be performed at such high Reynolds numbers. Self-generation of a magnetic field from turbulent velocity fluctuations when the measured mean flow alone is not a dynamo, is also a great experimental challenge.

3. Scalings for the saturation magnetic field close to the dynamo threshold. The expressions concerning the saturation magnetic field reported in this section are derived in details in [22]. In the following, we recall the main results in order to compare them with the experimental results of the Karlsruhe and Riga experiments. Our goal is to find the expression of the saturation magnetic field B as a function of ρ, ν, μ_0, σ, L and U. We have three independent parameters, Rm, Pm and, for instance, the square of the Lundquist number, $B^2\mu_0(\sigma L)^2/\rho$, thus we have in general

$$\frac{B^2\mu_0(\sigma L)^2}{\rho} = f(\mathrm{Rm}, \mathrm{Pm}). \tag{8}$$

Different scaling laws have been found for B using mean-field electrodynamics [12, 13, 14] or perturbation theory close to the dynamo threshold for laminar flows [13, 15, 16, 17, 18, 19, 20]. We will show that the two above assumptions (i) and (ii) can be used to find the scaling law for the realistic situation of a turbulent dynamo close to threshold: (i) implies that the momentum is mostly transported by turbulent fluctuations. Consequently, using the basic assumption of fully developed turbulence, we can neglect the kinematic viscosity, thus Pm. (ii) implies that the dependence of B^2 on Rm is proportional to $\mathrm{Rm}-\mathrm{Rm_c}$, as expected for a supercritical bifurcation close to the threshold. In other words, U is not a free parameter anymore, but should take approximately the value corresponding to the dynamo threshold. Thus, (i) and (ii) reduce the number of parameters from 6 to 4, and for the saturation value of the magnetic field we obtain, using the dimensional analysis,

$$B^2 \propto \frac{\rho}{\mu_0(\sigma L)^2}\,(\mathrm{Rm} - \mathrm{Rm_c}). \tag{9}$$

There is no paradox in the fact that the saturation magnetic field is inversely proportional to the electric conductivity and to the typical lengthscale of the flow. This does not mean that one should have σ and L small in order to observe large values of B since $\mathrm{Rm} = \mathrm{Rm_c}$ will be then achieved for a larger flow velocity. Using the typical velocity U_c at the dynamo threshold, we can write (9) in the form of $B^2/\mu_0\rho U_c^2 \propto (\mathrm{Rm} - \mathrm{Rm_c})/\mathrm{Rm_c^2}$, which shows that the system is very far from equipartition of magnetic and kinetic energy in the vicinity of the dynamo threshold. We emphasize also that the interaction parameter, i. e., the ratio of the Lorentz force to the pressure force driving the flow is much smaller than unity.

We have understood the above "turbulent scaling" together with the very different one obtained for $\mathrm{Pm} \gg 1$, by looking at the structure of the perturbative analysis describing the saturation of the magnetic field above the dynamo threshold [22]. For $\mathrm{Pm} \ll 1$, a lot of hydrodynamic bifurcations occur first and the flow becomes turbulent before reaching the dynamo threshold. Therefore, the perturbative calculation of the saturation field is tractable only for $\mathrm{Pm} \gg 1$ in general such that the dynamo bifurcates from a laminar flow. In the case of a

Ponomarenko type flow, we have obtained

$$B^2 \propto \frac{\rho\nu}{\sigma L^2}\,(\mathrm{Rm} - \mathrm{Rm_c}). \tag{10}$$

We call (10) the "laminar scaling", characterized by the fact that $B \to 0$ as $\nu \to 0$ with all the other parameters being fixed. This traces back to the fact that the Lorentz force is balanced by the viscous force corresponding to the perturbed velocity field. For $\mathrm{Pm} \ll 1$, we recover the "turbulent scaling" (9) if we balance the Lorentz force with the inertial terms in (4). We have $B_{laminar} \propto B_{turbulent}\,\mathrm{Pm}^{1/2}$, and the two scalings strongly differ for the experiments using liquid metals ($\mathrm{Pm} < 10^{-5}$).

It appears clearly that the saturation magnetic fields of order 10 mT roughly 10% above threshold observed in both the Karlsruhe [5] and Riga [6] experiments are in agreement with the "turbulent scaling" and in strong disagreement with the laminar one. Indeed, both experiments use liquid sodium ($\mu_0\sigma \sim 10\,\mathrm{m}^{-2}.\,\mathrm{s}$, $\rho \sim 10^3\,\mathrm{kg}.\,\mathrm{m}^{-3}$) and the inner diameter of the swirling flow channel in the Riga experiment as well as the period length of the flow used in the Karlsruhe experiment are of the same order of magnitude $L \sim 0.25\,\mathrm{m}$. We thus note that both experiments display a very interesting feature: turbulent fluctuations can be neglected when compute the dynamo threshold, but turbulence has a very strong effect on the value of the saturation magnetic field above the dynamo threshold.

In the case of rapidly rotating flows, the Lorentz force may be dominantly balanced by the Coriolis force corresponding to the perturbed velocity field. For the saturation magnetic field in the vicinity of threshold we obtain

$$B^2 \propto \frac{\rho\Omega}{\sigma}\,(\mathrm{Rm} - \mathrm{Rm_c}). \tag{11}$$

To conclude this section, we emphasize that the correct evaluation of the dominant transport mechanism for momentum is essential to estimate the order of magnitude of the saturation magnetic field above the dynamo threshold. The reason is that it determines the flow distortion by the Lorentz force and thus the saturation mechanism of the field. A mean field laminar model of the flow may thus lead to a wrong estimate of the field although it correctly predicts the dynamo threshold in the case of geometrically constrained flows. It would be interesting to test the validity of the scaling law (9) experimentally by varying the temperature of liquid sodium and thus its conductivity σ. Another fundamental experiment in the context of the geodynamo would be to observe the transition from (9) to (11) for a rapidly rotating flow.

4. Dynamics of the magnetic field close to the dynamo threshold. Magnetic fields of astrophysical objects are found to be almost time-periodic like that of the Sun, or nearly stationary, i.e., very slowly varying like for the Earth's magnetic field between two successive reversals. Although the solar dynamo may be far above the threshold, it is tempting to connect these temporal behaviors with the nature of the dynamo bifurcation, which can be either a stationary bifurcation or a Hopf bifurcation in the simplest generic cases. It should be noted that both the stationary bifurcation (Karlsrhue experiment), and the Hopf bifurcation (Riga experiment) have been observed so far. With these geometrically simple flows it is possible to guess the nature of bifurcation using symmetry considerations. This is less obvious in the case of a fully developed turbulent flow for which it would be interesting to try to understand how the dynamical regime above the dynamo onset is determined. In particular, a central problem in the context of geodynamo is to understand the mechanism of field reversals. Is it realistic to describe them

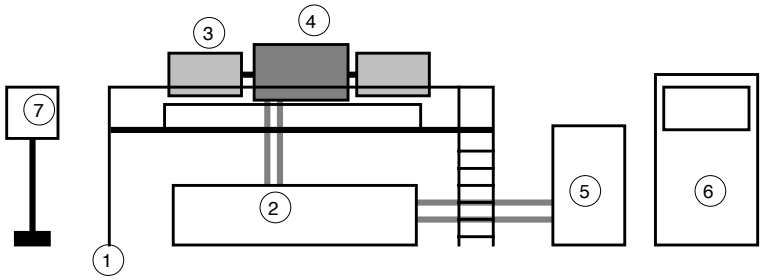

Fig. 1. Sodium loop. *1* – experimental platform, *2* – sodium tank (270 liters), *3, 4* – motors and flow vessel, *5* – sodium purifying unit, *6* – control unit, *7* – argon circuit command.

with low-dimensional dynamical systems [32] or are turbulence and unconstrained flows essential to generate them?

Such large scale dynamics have not been observed so far in the Karlsruhe and Riga experiments but both display small scale fluctuations of the magnetic field. An interesting feature is that some statistical properties of the fluctuations measured in the Karlsruhe experiment are similar to the ones observed in turbulent von Kármán flows in gallium [33] and sodium [24] below the dynamo threshold under an externally applied magnetic field. It would be of interest to understand whether this is because the field fluctuations measured in the Karlsruhe experiment are simply due to advection of the self-generated large scale magnetic field by the small-scale turbulent fluctations of the flow. This hypothesis would lead to a much simpler problem of advection of a passive vector field by a turbulent flow than in case these fluctuations were more deeply connected to the generation process itself.

5. The VKS experiment. On the premises of the CEA-Cadarache, we have built a versatile sodium facility that allows various flow configurations. Its main components are shown in Fig. 1. A sodium purification unit allows to operate at low temperature. Two 75 kW electric motors can generate flows in a volume of maximum 300 liters of sodium.

The first flow configuration corresponds to the von Kármán geometry: it is generated inside a cylindrical vessel with both diameter $2R$ and length H equal to 40 cm – see the sketch in Fig. 2 and [34, 24]. Two coaxial counter-rotating impellers generate the flow; they are driven by two 75 kW motors with rotation rates adjustable in the range of $f \in [0, 35]$ Hz. The maximum value is set by the maximum flow power consumption and depends on the shape of the impellers. Four longitudinal baffles (2 cm thick) can be mounted on the inner wall of the cylindrical vessel.

The kinetic Reynolds number Re of the flow is of the order of 10^6, so that turbulence is fully developed. One thus expects that both the velocity field and the magnetic field evolve over a large range of length and time scales. The hydrodynamic characteristics are obtained through measurements of the pressure fluctuations at the wall and of the flow power consumption. The pressure is recorded using a piezoelectric transducer mounted flush with the cylindrical wall; its rms amplitude yields the rms amplitude of velocity fluctuations [35, 36]:

$$p_{rms} \sim \frac{1}{2}\rho u_{rms}^2. \tag{12}$$

One obtains an rms velocity of about 45% of the driving discs rim speed. The power consumption of the flow is obtained from current and voltage in the driving

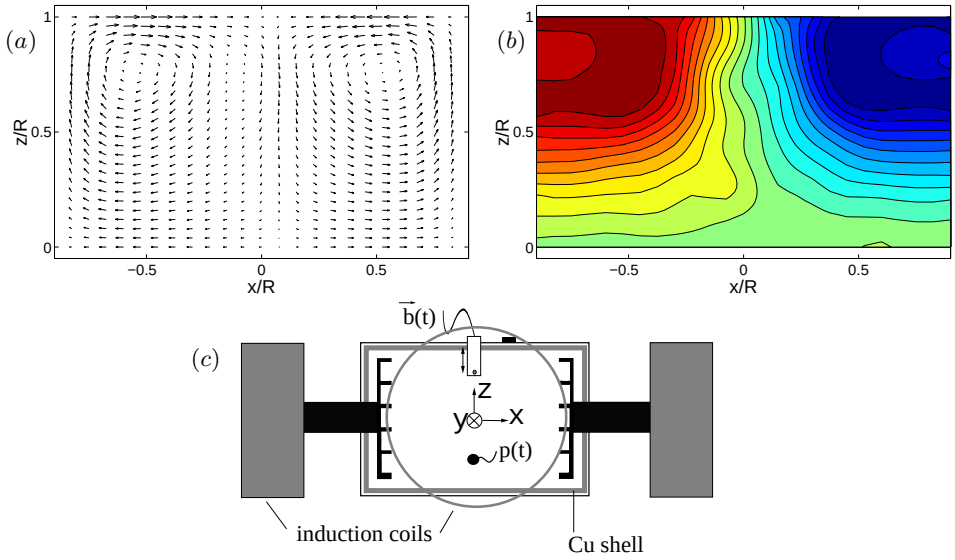

Fig. 2. Experimental set-up. Poloidal (a) and toroidal (b) components of the time averaged velocity profile in the counter-rotating von Kármán flow measured from LDV in a prototype water experiment with dics of 38 cm diameter and curved blades [42]. The abscissa corresponds to the normalized axial direction with the discs located at $x/R = \pm 0.9$, and the ordinate corresponds to the normalized radial direction (with $z/R = 0$ at the center of the discs). (c): principle of measurement of the response to an externally applied magnetic field. Two pairs of Hemoltz induction coils have their axis (horizontal) aligned either parallel to the rotation axis or perpendicular to it. They can produce an applied field of about 20 G inside the flow. The magnetic field is measured locally *in situ* using a Hall probe located at the intersection between the vertical meridian plane and the median plane. Its depth inside the flow is adjustable. The (x, y, z) coordinates shown give the local orientation of the field components measured by the magnetic probe.

motors or from the temperature drift inside the flow when the external cooling is turned off. In agreement with the dimensional argument for turbulent flows [36], we observe for discs of 38 cm diameter with curved blades and no baffles [24]:

$$P = K_P \, \rho R^5 \Omega^3 \quad , \tag{13}$$

where $\Omega = 2\pi f$ is the angular velocity and $K_P = 0.14$. The knowledge of P yields an estimate of the hydrodynamic dissipation scale η:

$$\eta \sim \left(\frac{\nu^3}{P/\rho \mathcal{V}} \right)^{1/4} \sim 5 \, \mu\text{m} \quad , \tag{14}$$

where $\mathcal{V}$ is the volume. The Taylor microscale λ, i.e., the scale, at which the turbulent velocity gradients are the largest, is estimated from

$$\lambda \sim \left(\nu \, \frac{u_{rms}^2}{P/\rho \mathcal{V}} \right)^{1/2} \sim \left(\nu \, \frac{p_{rms}}{P/\mathcal{V}} \right)^{1/2} \sim 200 \, \mu\text{m} \quad , \tag{15}$$

These values must be compared to the diffusive length scale ℓ_B of the magnetic field

$$\ell_B \sim \left(\frac{1}{\mu_0 \sigma \Omega} \right)^{1/2} \sim 10 \text{ cm}. \tag{16}$$

One thus expects that the dynamics of the magnetic field is dominated by the largest scales of the flow.

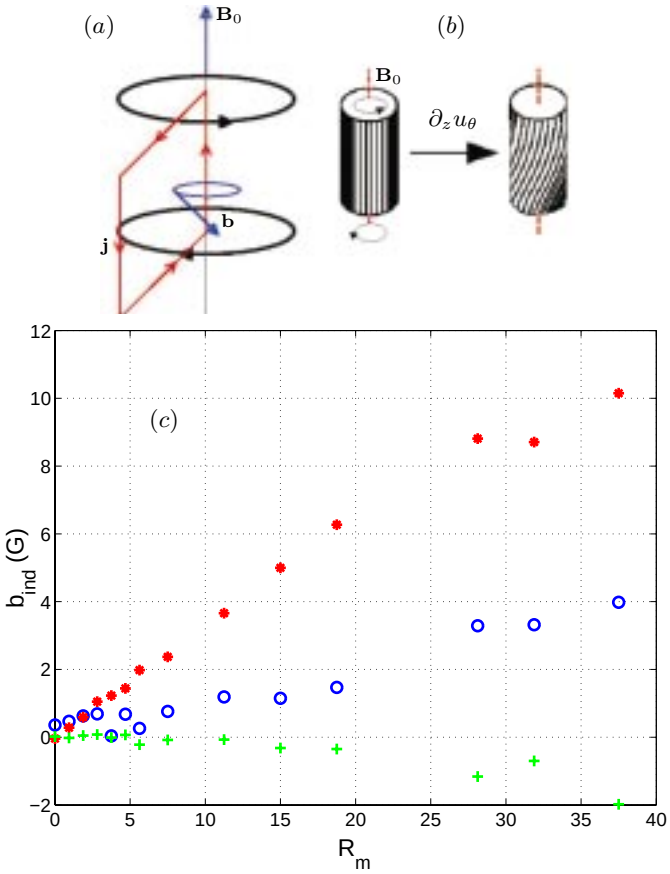

Fig. 3. Ω effect. (*a*): sketch of the induction mechanims and induced currents; (*b*): corresponding distorsion of axial magnetic field lines; (*c*): response to an applied axial field $B_0 = 5.4$ G, in the case of two counter-rotating discs. The induced field $\mathrm{b_{ind}}$ is measured inside the flow, in the mid-plane, 4 cm from the rotation axis. Its 3 components are plotted vs the magnetic Reynolds number Rm: (○) axial component b_x, (∗) transverse component b_y, (+) vertical component b_z. The disc diameter is 30 cm with eight curved blades and four baffles mounted on the inner wall of the cylindrical vessel.

6. Large scale induction effects.

6.1. Induction by the mean flow. A detailed analysis of the response of the von Kármán swirling flow to an externally applied magnetic field has been presented in other publications [34, 24]. Here we discuss the induction in von Kármán swirling flows with regards to the possibility of dynamo self-generation in such a flow geometry. We first consider the induction by the mean flow motion, i.e., by the time-averaged flow profile. A possible dynamo instability mechanism is the following: let $\mathbf{b}_0$ be an initial magnetic field fluctuation in the flow; the flow motion will generate an induced component $\mathbf{b}_1$, which, being combined to the flow motion, generates in turn an induced component $\mathbf{b}_2$, etc. The dynamo action is reached if at some point ($\mathrm{Rm} > \mathrm{Rm_c}$), $\mathbf{b}_n$ reinforces $\mathbf{b}_0$ so that the net magnetic field grows. In this laminar picture, two hydrodynamic features have been shown to play a fundamental role [10]: differential rotation and helicity. They are at the heart of the laminar, geometrically constrained, dynamos in the Riga [6] and Karlsruhe [5] experiments. Helicity and differential rotation are also present in the counter-rotating von Kármán flows, as shown in Fig. 2. The opposite rota-

tions of the discs create a strong differential rotation in the mid-plane of the flow. In addition, the rotating discs act as centrifugal fans: they produce the rotation and pump the fluid near the axis; the resulting swirling motion possesses a strong helicity.

6.2. Ω and α effects. To study the magnetic induction in this flow, we placed coils with their axis either aligned with the rotation axis of the two motors, or perpendicular to it – see Fig. 2. In this way, we can apply a field, $\mathbf{B}_0$, either parallel or perpendicular to the rotation axis. Its amplitude is of the order of 20 G and does not modify the flow – the interaction parameter is of the order of $N \sim 10^{-3}$. We measure the three components of the field induced by a local magnetic probe located inside the flow; we use a calibrated and temperature-compensated 3D Hall probe (F.W. BELL) with a dynamical range of 65 dB and a time resolution of 20 μs. We present, in the following, the results obtained with discs of 30 cm diameter with curved blades and baffles.

When the (almost uniform) external field is applied along the rotation axis (poloidal), the main induced field component is toroidal. This effect is known as the Ω effect [10]. It can be viewed as a result of the axial magnetic field lines twisting by the differential rotation of the flow or as a result of the generation of poloidal currents cf. Fig. 3*a*, *b*. Fig. 3*c* shows the three components of the local induced field measured in the median plane and 10 cm away from the rotation axis, when an external axial field is applied. As expected, the main effect is the generation of a toroidal component. Note that the amplitude of this induced component exceeds that of the applied field as Rm becomes larger than about 17.

The effect of helicity is best demonstrated when the flow is driven by the rotation of a single disc [37]. The mean flow is made of a toroidal rotation and a single poloidal recirculation loop. In the center of the cylinder, the fluid has a spiraling motion towards the rotating disc. As sketched in Fig. 4(a), when an external field $\mathbf{B}_0$ is applied perpendicularly to the axis of the helical motion, a current parallel to $\mathbf{B}_0$ is generated. This is a macroscopic equivalent of the α effect proposed by Parker [38], Krause and Rädler [9], which is at the heart of the Karlsruhe dynamo [5]. The 'α current' generates an axial magnetic field; as shown in Fig. 4(b), it can also be understood as resulting from the distortion of transverse magnetic field lines by the helical motion. The measurement reported in Fig. 4(c) is made in the case of a single rotating disc; the induced field is recorded as a function of the magnetic Reynolds number in the mid-plane of the flow. One observes that the axial field component $\langle B_x \rangle$ varies quadratically with Rm, for Rm < 10 being in agreement with the two-step α mechanism; its sign is determined by those of $\mathbf{B}_0$ and of helicity $\mathbf{v}.(\nabla \times \mathbf{v})$. For comparison, the vertical component $\langle B_z \rangle$ varies linearly with Rm, as expected in this range of Rm. We have also observed that as the rotation rate of the disc increases, the transverse field is progressively expelled from the core of the spiraling motion [37]. This expulsion of the magnetic field from eddies is well documented, both theoretically [39] and experimentally [40]. We now turn to the case when both discs are counter-rotating, and we first note that in the core of the flow the helicities near each disc have the same sign. Indeed, near each disc the direction of rotation is reversed, but so is the axial flow towards the disc. One can thus expect that both the large scale α effect and the Ω effect may occur in this flow geometry. This can be probed by applying an external field perpendicular to the axis of rotation. In this case, one expects that the axial component of the induced magnetic field $\langle B_x \rangle$ results mainly from the α effect and that a transverse component $\langle B_y \rangle$ results from the action of differential rotation on $\langle B_x \rangle$, i.e., an $\alpha\Omega$ effect. As shown in Fig. 5, this is partially correct: the transverse component $\langle B_y \rangle$ demonstrates a non linear behavior, indeed well represented by a

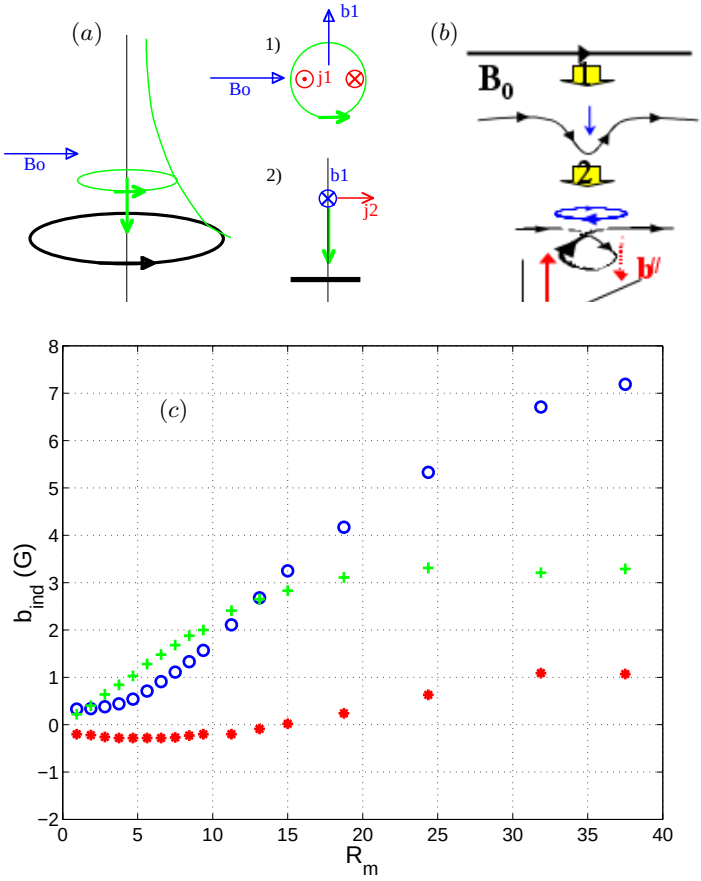

Fig. 4. α effect in the case of a single rotating disc (the same disc as in Fig. 3). (a): sketch of the induction mechanisms and induced currents; (b): corresponding distortion of transverse magnetic field lines; (c): response to an applied field perpendicular to the rotation axis, $B_0 = 9$ G. The induced field b_{ind} is measured inside the flow, in the mid-plane, 4 cm from the rotation axis. Its 3 components are plotted vs the magnetic Reynolds number Rm: ($\circ$) axial component b_x, ($*$) transverse component b_y, ($+$) vertical component b_z.

cubic scaling in Rm (for Rm < 30), consistent with a three-step mechanism such as the $\alpha\Omega$ effect. However, the axial component $\langle B_x \rangle$ does not vary quadratically, although we have verified by varying the direction of rotation of the discs that its direction is given by those of $\mathbf{B}_0$ and of helicity $\mathbf{v} \cdot (\nabla \times \mathbf{v})$.

Finally, we note that whenever the flow is produced by the counter-rotation of the driving discs, the level of turbulence in the flow is very high. As a result, large fluctuations in the induced magnetic field are also observed [24]; for instance, in the data reported in Figs 3 and 5, the variance of the magnetic field components is of the order of 50% of the mean.

6.3. Discussion. Our experimental measurements of induction in the presence of an externally applied magnetic field show the existence of large scale α and Ω effects in our flow geometry. Our measurements are also consistent with the $\alpha\Omega$ induction effects, that underlies the kinematic dynamo observed numerically in this geometry [41, 42]. This possibility of a kinematic dynamo has motivated an extensive optimization procedure to define the driving mechanism and

the electrical boundary conditions [34, 42]: the shape of the impellers has been designed to generate poloidal and toroidal velocities of the same order of magnitude ($P/T \simeq 0.8$) and the stainless steel vessel has been fitted with an inner copper wall (1 cm thick). The kinematic dynamo threshold corresponding to these impellers ranges from 130 for insulating boundaries to 70 for a layer of sodium at rest (thickness equal to 4 cm) surrounding the moving fluid [42]. However, although we have observed that the mean local axial and transverse induction are larger than unity, we have not observed self-generation. In the following, we venture some (non exhaustive and non mutually exclusive) explanations.

First, the maximum magnetic Reynolds Rm^{max} reached in the experiment remains under $\mathrm{Rm_c}$. However, the kinematic dynamo calculations performed on the mean flow show that Rm^{max} should be very close to $\mathrm{Rm_c}$. Accordingly, we could expect an increase of the induced magnetic field associated with the threshold vicinity. On the contrary, we observe a saturation of the induced field when increase Rm, that is difficult to understand.

Another possibility is that although an $\alpha\Omega$ process sets in at low Rm, it is progressively quenched at higher Rm values because of the expulsion of the transverse field component by the axial eddies of the mean flow. This would be consistent with saturation of the induction, as observed in Figs. 3, 4 and 5 at large values of Rm.

One possibility is that the actual dynamo threshold in the experiment is much larger than the one calculated in the kinematic simulation. It is very hard to experimentally reproduce an optimized configuration, and the kinematic dynamo studies [41, 42] show that the threshold is very sensitive to fine details in the flow geometry: the ratio of poloidal to toroidal velocities, the position of zeros of poloidal velocities and maximum of toroidal velocities, etc. Surprisingly, small

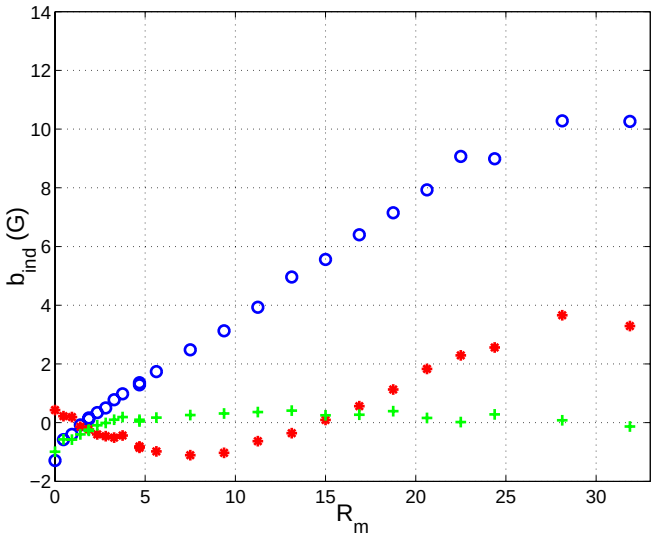

Fig. 5. Response to a transverse applied field in the case of two counter-rotating discs (the same configuration as in Fig. 3). The externally applied field $B_0 = 9$ G is perpendicular to the rotation axis. The induced magnetic field $\mathbf{b}_{\mathrm{ind}}$ is measured in the mid plane, at a distance of 4 cm from the rotation axis. Its 3 components are plotted vs the magnetic Reynolds number Rm: ($\circ$) axial component b_x, ($*$) transverse component b_y, ($+$) vertical component b_z.

variations in the flow geometry can increase the critical magnetic Reynolds number by a factor of 2, or even cancel the bifurcation.

The above argument becomes quite meaningful if one recalls that the experimental flow field has strong fluctuations of the order of 50% of the mean velocity. This makes the very concept of the mean flow (average over time of the velocity profiles) quite suspicious. In the actual experiment, the large scale geometry varies in time and thus deeply affects the magnetic induction. This point of view explains the observed fluctuations of induction (figures above) and is consistent with the observed large scale correlations between the induction and the pressure fluctuations at the flow wall [34, 24]. In this picture, instantaneous fluctuations of the flow topology may prevent an in-phase cooperative mechanism. Fluctuations in flow topology could change the geometry of the neutral mode faster than the instability develops.

In conclusion, many open questions remain for the problem of homogeneous turbulent dynamos. New experimental campaigns are planned in this direction with the VKS facility.

Acknowledgments. We gratefully acknowledge the technical assistance of J.-B. Luciani, F. Namer, A. Guigon, M. Moulin, C. Gasquet, V. Padilla and D. Ericher and the financial support of the French institutions: Commissariat à l'Energie Atomique, Ministère de la Recherche and Centre National de la Recherche Scientifique.

REFERENCES

1. A. Herzenberg. Geomagnetic dynamos. *Philos. Trans. Roy. Soc. London* A, vol. 250 (1958), p. 543.
2. D. Lortz. Exact solution of the hydromagnetic dynamo problem. *Plasma Phys.*, vol. 10 (1968), p. 967.
3. G.O. Roberts. Dynamo action of fluid motions with two-dimensional periodicity. *Phil. Trans. Roy. Soc. London* A, vol. 271 (1972), p. 411.
4. Yu.B. Ponomarenko. Theory of the hydromagnetic generator. *J. Appl. Mech. Tech. Phys.*, vol. 14 (1973), p. 775.
5. R. Stieglitz, U. Müller. Experimental demonstration of a homogeneous two-scale dynamo. *Phys. Fluids*, vol. 13 (2001), pp. 561–564.
6. A. Gailitis, O. Lielausis, E. Platacis, S. Dement'ev, A. Cifersons, G. Gerbeth, Th. Gundrum, F. Stefani, M. Christen, G. Will Magnetic field saturation in the Riga dynamo experiment. *Phys. Rev. Lett.*, vol. 86 (2001), pp. 3024–3027.
7. K.-H. Rädler, E. Apstein, M. Rheinhardt, M. Schüler. The Karlsruhe dynamo experiment. A mean-field approach. *Studia geoph. et geod.*, vol. 42 (1998), pp. 224–231.
8. F.H. Busse, U. Müller, R. Stieglitz, A. Tilgner. Spontaneous generation of magnetic fields in the laboratory. In *Evolution of Spontaneous Structure in Dissipative Continuous Systems* (ed. F.H. Busse and S.C. Müller), Springer 1998, pp. 546–558.
9. F. Krause, K.-H. Rädler. *Mean-Field Magnetohydrodynamics and Dynamo Theory.* Akademie–Verlag, Berlin and Pergamon Press, Oxford (1980).
10. H.K. Moffatt. *Magnetic Field Generation in Electrically Conducting Fluids*, Cambridge University Press (Cambridge 1978).
11. K.-H. Rädler, M. Rheinhardt, E. Apstein, H. Fuchs. On the mean-field theory of the Karlsruhe dynamo experiment. *Nonlinear Processes in Geophysics*, (2002) in print.

12. M. Meneguzzi, U. Frisch, A. Pouquet. Helical and nonhelical turbulent dynamos. *Phys. Rev. Lett.*, vol. 47 (1981), p. 1060.

13. A.D. Gilbert, P.L. Sulem. On inverse cascades in alpha effect dynamos. *GAFD*, vol. 51 (1990), p. 243.

14. A.V. Gruzinov, P.H. Diamond. Self-consistent theory of mean-field electrodynamics. *Phys. Rev. Lett.*, vol. 72 (1994), p. 1651.

15. S. Childress, A.M. Soward. Convection-driven hydromagnetic dynamo. *Phys. Rev. Lett.*, vol. 29 (1972), p. 837.

16. A.M. Soward. A convection driven dynamo. I. The weak field case. *Phil. Trans. R. Soc. Lond.* A, vol. 275 (1974), p. 611.

17. F.H. Busse. Generation of planetary magnetism by convection. *Phys. Earth Planet. Inter.*, vol. 12 (1976), pp. 350–358.

18. Y. Fauterelle,S. Childress. Convective dynamos with intermediate and strong fields. *GAFD*, vol. 22 (1982), p. 235.

19. A.P. Bassom, A.D. Gilbert. Nonlinear equilibration of a dynamo in a smooth helical flow. *J. Fluid Mech.*, vol. 343 (1997), p. 375.

20. A. Nunez, F. Pétrélis and S. Fauve Saturation of a Ponomarenko type fluid dynamo. *Dynamo and Dynamics, a Mathematical Challenge*, Eds P. Chossat *et al.* Kluwer Acad. Publ., 2001, pp. 67–74.

21. A. Tilgner, F.H. Busse. Saturation mechanism in a model of the Karlsruhe Dynamo. *Dynamo and Dynamics, a Mathematical Challenge*, Eds P. Chossat *et al.* Kluwer Acad. Publ., 2001, pp. 109–116.

22. F. Pétrélis, S. Fauve. Saturation of the magnetic field above the dynamo threshold. *Eur. Phys. J.* B, vol. 22 (2001), p. 273.

23. N.L. Peffley, A.B. Cawthrone, D.P. Lathrop. Toward a self-generating magnetic dynamo: The role of turbulence. *Phys. Rev.* E, vol. 61 (2000), p. 5287. .

24. M. Bourgoin, L. Marié, F. Pétrélis, C. Gasquet, A. Guigon, J.-B. Luciani, M. Moulin, F. Namer, J. Burguete, A. Chiffaudel, F. Daviaud, S. Fauve, P. Odier, J.-F. Pinton. MHD measurements in the von Kármán sodium experiment. To appear in *Phys. Fluids* (2002).

25. U. Frisch. *Turbulence*, Cambridge University Press (Cambridge 1995).

26. T. John, R. Stannarius, U. Behn. On-Off Intermittency in Stochastically Driven Electrohydrodynamic Convection in Nematics. *Phys. Rev. Lett.*, vol. 83 (1999), p. 749.

27. R. Berthet, A. Petrossian, S. Residori, B. Roman, S. Fauve. Effect of multiplicative noise on parametric instabilities. Submitted to *Phyica* D (2001).

28. D. Sweet, E. Ott, J. Finn, T. M. Antonsen, D. Lathrop. Blowout bifurcations and the onset of magnetic activity in turbulent dynamos. *Phys. Rev.* E, vol. 63 (2001), p. 66211.

29. A. B. Reighard, M. R. Brown,. Turbulent Conductivity Measurements in a Spherical Liquid Sodium Flow. *Phys. Rev. Lett.*, vol. 86 (2001), p. 2794.

30. A. Lanotte, A. Noullez, M. Vergassola, A. Wirth. Large scale dynamo by negative magnetic eddy diffusivities. *Geophys. Astrophys. Fluid Dynamics*, vol. 91 (1999), p. 131.

31. V.A. Zheligovsky, O.M. Podvigina, U. Frisch. Dynamo effect in parity invariant flow with large and moderate separation of scales. *Geophys. Astrophys. Fluid Dynamics*, vol. 95 (2001), pp. 227–268.

32. T. Rikitake. Oscillations of a system of discs dynamos. *Proc. Camb. Phil. Soc.*, vol. 54 (1958), pp. 89–105.

33. P. Odier, J.-F. Pinton, S. Fauve. Advection of a magnetic field by a turbulent swirling flow. *Phys. Rev.* E, vol. 58 (1998), pp. 7397–7401.

34. L. Marié, J. Burguete, A. Chiffaudel, F. Daviaud, D. Ericher, C. Gasquet, F. Pétrélis, S. Fauve, M. Bourgoin, M. Moulin, P. Odier, J.-F. Pinton, A. Guigon, J. B. Luciani, F. Namer, J. Léorat. MHD in von Kármán swirling flows, development and first run of the Sodium experiment. In *Dynamo and Dynamics, A Mathematical Challenge*, Cargèse (France), August 21-26, 2000. P. Chossat *et al.* (eds.) *Kluwer Academic Publishers* (2001).

35. S. Fauve, C. Laroche, B. Castaing. Pressure fluctuations in swirling turbulent flows. *J. Phys. II*, vol. 3 (1993), p. 271.

36. N. Mordant, J.-F. Pinton, F. Chillà. Characterization of turbulence in a closed flow. *J. Phys. II*, vol. 7 (1997), pp. 1–12.

37. F. Pétrélis, L. Marié, M. Bourgoin, A. Chiffaudel, F. Daviaud, S. Fauve, P. Odier, J. -F. Pinton. The alpha effect and its saturation in a turbulent swirling flow generated in the VKS experiment. submitted to *Phys. Rev. Lett.* (2001).

38. E.N. Parker, "Hydromagnetic dynamo models". *Astrophysical J.*, vol. 122 (1955), p. 293.

39. N.O. Weiss. The expulsion of magnetic flux by eddies. *Proc. Roy. Soc.* A, vol. 293 (1966), p. 310. .

40. P. Odier, J.-F. Pinton, S. Fauve. Magnetic induction by coherent vortex motion. *Eur. Phys. J. B*, vol. 16 (2000), p. 373. .

41. J. Léorat. A new experimental project of fluid dynamo. *Proc. Pamir Conference*, Aussois (France), (1998).

42. J. Burguete, L. Marié, F. Daviaud, J. Léorat. Homogeneous dynamo: numerical analysis of experimental von Kármán type flows. Submitted to *Eur. Phys. J. B.* (2002).

Received 19.10.2001